

# Robust Interlayer Exciton in WS<sub>2</sub>/MoSe<sub>2</sub> van der Waals Heterostructure under High Pressure

Xiaoli Ma,<sup>▽</sup> Shaohua Fu,<sup>▽</sup> Jianwei Ding,<sup>▽</sup> Meng Liu,<sup>▽</sup> Ang Bian, Fang Hong,\* Jiatao Sun,\* Xiaoxian Zhang,\* Xiaohui Yu,\* and Dawei He

Cite This: *Nano Lett.* 2021, 21, 8035–8042

Read Online

ACCESS |

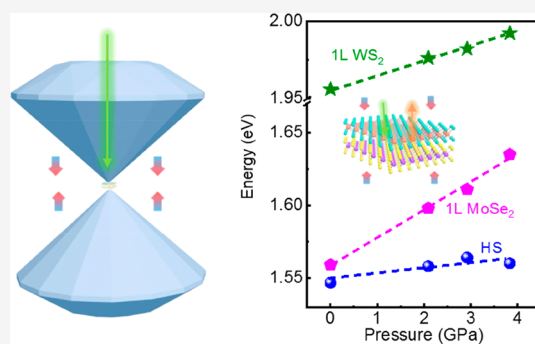
Metrics & More

Article Recommendations

Supporting Information

**ABSTRACT:** The van der Waals (vdW) heterostructures have rich functions and intriguing physical properties, which has attracted wide attention. Effective control of excitons in vdW heterostructures is still urgent for fundamental research and realistic applications. Here, we successfully achieved quantitative tuning of the intralayer exciton of monolayers and observed the transition from intralayer excitons to interlayer excitons in WS<sub>2</sub>/MoSe<sub>2</sub> heterostructures, via hydrostatic pressure. The energy of interlayer excitons is in a “locked” or “superstable” state, which is not sensitive to pressure. The first-principles calculation reveals the stronger interlayer interaction which leads to enhanced interlayer exciton behavior in WS<sub>2</sub>/MoSe<sub>2</sub> heterostructures under external pressure and reveals the robust peak of interlayer excitons. This work provides an effective strategy to study the interlayer interaction in vdW heterostructures and reveals the enhanced interlayer excitons in WS<sub>2</sub>/MoSe<sub>2</sub>, which could be of great importance for the material and device design in various similar quantum systems.

**KEYWORDS:** *van der Waals heterostructures, interlayer exciton, high pressure engineering, electronic coupling, band structure*

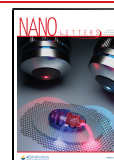


## INTRODUCTION

With the emergence of two-dimensional materials, monolayer transition metal dichalcogenides (TMDs) have attracted a wide range of scientific and engineering interest due to their unique electronic structure.<sup>1–5</sup> Recently, they have become an ideal platform to explore fundamental scientific problems in two-dimensional systems, as well as potential applications in optoelectronics because of the strong light–matter interactions.<sup>6–9</sup> In particular, two-dimensional (2D) TMDs with exotic properties such as an indirect-to-direct band gap transition in monolayers,<sup>10–12</sup> valley-selective optical coupling,<sup>13–15</sup> and large binding energies of excitons<sup>16–18</sup> have paved the way for studying the basic optical properties of the materials. Besides, with the development of the diverse transfer method, vdW heterostructures composed of different materials can be randomly stacked and attached together by vdW interaction,<sup>19–22</sup> which greatly broadened the exploration of exciton physics and thus provided more opportunities for future optoelectronic applications. Many fascinating physical phenomena have been reported in various vdW heterostructures, as exemplified by transport measurements revealing Hofstadter butterfly states, fractional Chern insulators, gate-tunable Mott insulators, and unconventional superconductivity, among other effects.<sup>23–29</sup> In addition, the existence of stable interlayer excitons and Moiré excitons has been reported in TMD heterostructures via tuning stacking angles.<sup>30,31</sup> Recently,

studies of WS<sub>2</sub>/MoSe<sub>2</sub> heterostructures showed that the nearly degenerate conduction-band edges with band offset calculated to be as small as 20 or 60 meV<sup>32,33</sup> can promote the formation of hybridized Moiré excitons due to the resonant enhancement of the hybridization strength and Moiré superlattice effects.<sup>31</sup> An intriguing problem is how to effectively tune the electronic structure and interlayer coupling or excitons of vdW heterostructures, which will lead to the observation of new exciton behavior. As reported previously, the coupling of the heterointerface can be tuned slightly by annealing in a high vacuum,<sup>34</sup> by inserting hexagonal BN dielectric layers into the vdW gap,<sup>35</sup> or by twisting the angle in 2D transition metal dichalcogenide semiconductors.<sup>36</sup> On the other hand, high pressure has been proven to be a powerful tool to change the electronic structure and even promote phase transition of materials in the past few years.<sup>37,38</sup> Intriguing physical phenomena such as pressure-induced direct–indirect band gap transition,<sup>38</sup> isostructural phase transition (2H<sub>c</sub> to 2H<sub>a</sub>),<sup>37,39</sup> and semiconductor-to-metal transition<sup>40,41</sup> have been success-

Received: June 11, 2021  
 Revised: September 28, 2021  
 Published: October 4, 2021



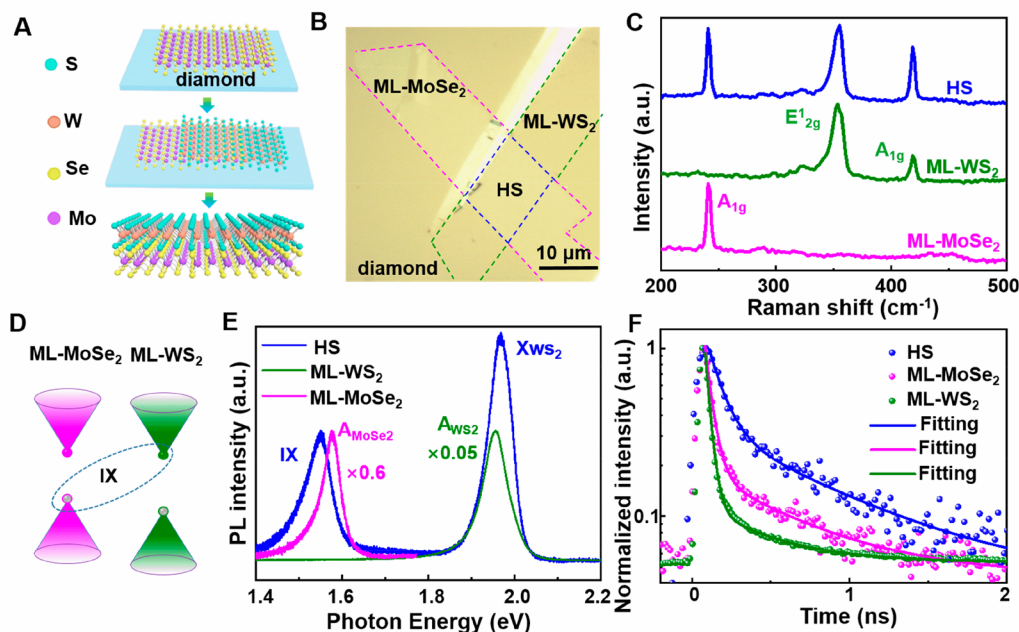


**Figure 1.** Construction and optical characterization of a ML-WS<sub>2</sub>/ML-MoSe<sub>2</sub> heterostructure. (A) Schematic diagram of a vertical WS<sub>2</sub>/MoSe<sub>2</sub> vdW heterostructure (HS). (B) Optical micrograph of the WS<sub>2</sub>/MoSe<sub>2</sub> heterostructure, fabricated by the dry transfer method. ML-MoSe<sub>2</sub>, ML-WS<sub>2</sub>, and heterostructure regions are marked by pink, green, and blue dashed lines, respectively. (C) Raman spectra of ML-MoSe<sub>2</sub>, ML-WS<sub>2</sub>, and WS<sub>2</sub>/MoSe<sub>2</sub> heterostructures, respectively. (D) Schematic illustration of the type-II band alignment of the WS<sub>2</sub>/MoSe<sub>2</sub> heterostructure and the formation of interlayer excitons. (E) PL spectra of an individual monolayer and the heterostructure. The new PL peak at 1.548 eV indicates the formation of interlayer excitons (IX). (F) Time-resolved PL decay curves for ML-MoSe<sub>2</sub>, ML-WS<sub>2</sub>, and WS<sub>2</sub>/MoSe<sub>2</sub> heterostructure.

fully observed in TMD systems. Since the optical property of TMD heterostructures is directly correlated with their electronic structures, this permits us to tune interlayer coupling and excitons in vdW heterostructures via external pressure. High-pressure tuning on the interlayer excitons of vdW heterostructures has rarely been reported, which may be due to the difficulty of fabricating high-quality samples inside the high-pressure chamber. However, it is essential to investigate the efficient tuning of the optical and optoelectronic properties of vdW heterostructures by high pressure in a quantitative way. Here, we chose to study the WS<sub>2</sub>/MoSe<sub>2</sub> heterostructure as an example by applying hydrostatic pressure via a diamond anvil cell (DAC) and observed the enhanced exciton behavior.

## RESULTS AND DISCUSSION

A high-quality WS<sub>2</sub>/MoSe<sub>2</sub> heterostructure has been constructed on the culet of diamond by the dry transfer method. A schematic illustration of the stacking process is shown in Figure 1A. Monolayer WS<sub>2</sub> (ML-WS<sub>2</sub>) is transferred onto monolayer MoSe<sub>2</sub> (ML-MoSe<sub>2</sub>) through the layer-by-layer dry transfer technique, as detailed in the Methods section (Figure S1). Since a high-quality interface is essential for charge transfer between two individual monolayer materials, the samples were annealed at 120 °C for 2 h under a vacuum. The interface between WS<sub>2</sub> and MoSe<sub>2</sub> is linked by weak vdW forces. Figure 1B presents the corresponding optical image of a WS<sub>2</sub>/MoSe<sub>2</sub> heterostructure on a diamond substrate. The layer number of the MoSe<sub>2</sub> and WS<sub>2</sub> region of interest has been identified by the contrast of the optical image, Raman spectrum, and PL spectrum. Figure 1C shows the Raman characteristic peaks of the out-of-plane A<sub>1g</sub> mode for ML-MoSe<sub>2</sub> (at 240 cm<sup>-1</sup>) and the out-of-plane A<sub>1g</sub> mode and in-plane E<sub>2g</sub> mode for ML-WS<sub>2</sub> (at 417 and 353 cm<sup>-1</sup>), and the heterostructure region clearly shows these three

distinguishable modes. The quality of the heterostructure is further examined by the Raman spectra. The A<sub>1g</sub> mode of WS<sub>2</sub> that is sensitive to layer thickness is greatly enhanced, which indicates the successful formation of the heterobilayer.<sup>42</sup>

To investigate the interlayer electronic coupling and interlayer excitons in our heterostructure, we performed micro-PL measurements of ML-MoSe<sub>2</sub>, ML-WS<sub>2</sub>, and the WS<sub>2</sub>/MoSe<sub>2</sub> heterostructure (Figure 1E). The monolayer samples showed emission peaks at ~1.577 and ~1.955 eV, which corresponds to the direct interband K–K transition of the A excitons of ML-MoSe<sub>2</sub> (A<sub>MoSe<sub>2</sub></sub>) and ML-WS<sub>2</sub> (A<sub>WS<sub>2</sub></sub>), respectively. For the heterostructure region, an additional emission peak at ~1.548 eV that has lower energy than the A exciton of MoSe<sub>2</sub> is observed, beyond the emission peak of the A exciton of WS<sub>2</sub> (X<sub>WS<sub>2</sub></sub>). According to recent reports,<sup>31,43</sup> this new peak can be assigned to the interlayer exciton (IX) of the WS<sub>2</sub>/MoSe<sub>2</sub> heterostructure, which is formed by the recombination of electrons and holes from different layers. At the same time, the PL intensity of WS<sub>2</sub> has been quenched about 7 times, indicating that masses of the holes generated in WS<sub>2</sub> were transferred to MoSe<sub>2</sub> before radiative recombination. To facilitate the comparison of the emission peak energy, we multiplied the PL intensity of ML-WS<sub>2</sub> (A<sub>WS<sub>2</sub></sub>) and ML-MoSe<sub>2</sub> (A<sub>MoSe<sub>2</sub></sub>) by coefficients of 0.05 and 0.6, respectively. The original figure was shown in Figure S2. It is easy to understand this phenomenon because the type-II band alignment<sup>44,45</sup> of the WS<sub>2</sub>/MoSe<sub>2</sub> heterostructure, depicted in Figure 1D, will facilitate the occurrence of charge transfer between the two layers. This type-II band alignment not only provides a direct channel for the interlayer coupling but also confirms the interlayer nature of the observed peak at ~1.548 eV. The absence of the A exciton peak of MoSe<sub>2</sub> from the overall PL spectrum is consistent with the previous reports,<sup>31,43</sup> suggesting

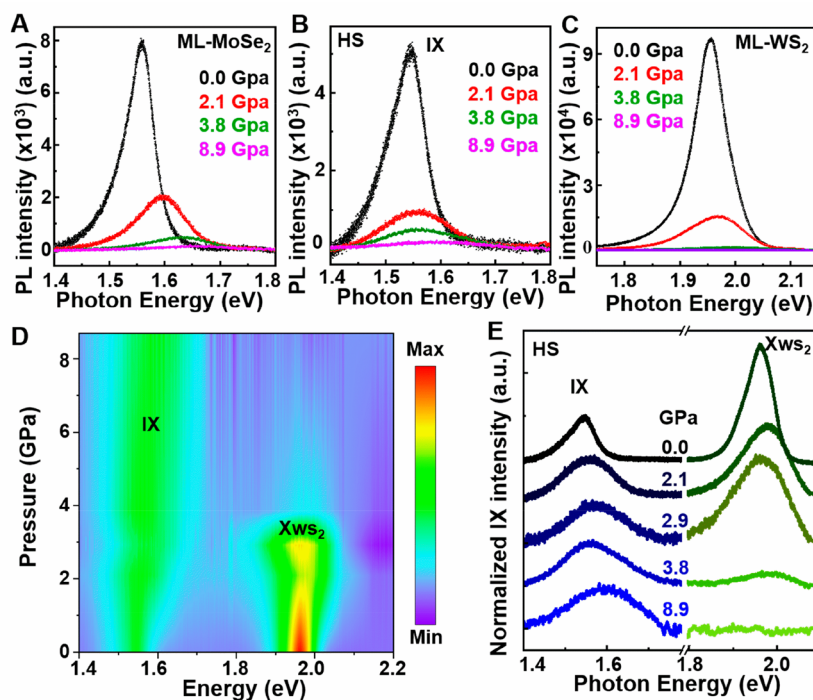


**Figure 2.** PL spectrum of ML-MoSe<sub>2</sub>, WS<sub>2</sub>/MoSe<sub>2</sub> heterostructure, and ML-WS<sub>2</sub> and normalized intensity of interlayer exciton peaks under different pressures. (A–C) PL spectrum of ML-MoSe<sub>2</sub>, WS<sub>2</sub>/MoSe<sub>2</sub> heterostructure, and ML-WS<sub>2</sub> under different pressures from 0 to 8.9 GPa, respectively. (D, E) Normalized intensity of interlayer exciton peaks under different pressures. As the pressure increases, the A exciton of WS<sub>2</sub>, which is the prominent emission at a pressure of nearly zero, is suppressed compared to the interlayer exciton (IX) emission in the heterostructure region.

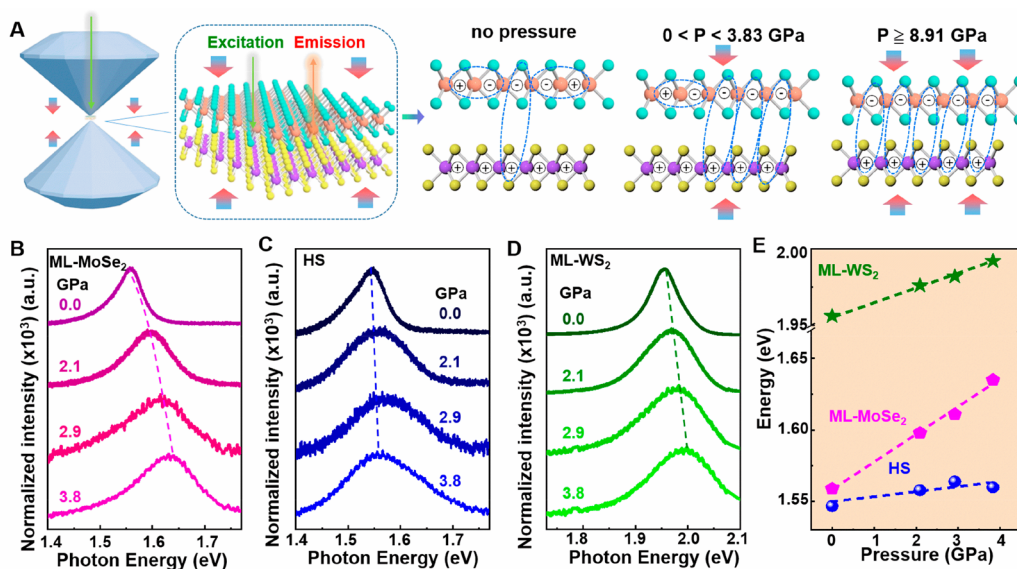


**Figure 3.** Pressure engineering of electronic structure and interlayer coupling in WS<sub>2</sub>/MoSe<sub>2</sub> heterostructure. (A) Schematic illustration of the transformation of interlayer and intralayer excitons in a vertical WS<sub>2</sub>/MoSe<sub>2</sub> vdW heterostructure, where hydrostatic pressure is applied through a DAC device. (B–D) Pressure-dependent PL spectra of ML-MoSe<sub>2</sub>, WS<sub>2</sub>/MoSe<sub>2</sub> heterostructure, and ML-WS<sub>2</sub>, respectively. PL spectra of monolayer regions are individually normalized to the peak of maximum intensity. In the heterostructure region, the intensity of interlayer exciton peaks is normalized to compare the coupling strength at varying pressures. (E) Photon energies of the PL peak  $A_{\text{MoSe}_2}$ ,  $A_{\text{WS}_2}$ , and IX as a function of pressure.

effective interlayer charge transfer across this heterostructure region.

In order to further confirm the formation of interlayer excitons, we performed time-resolved photoluminescence (TRPL) measurements at isolated WS<sub>2</sub>, MoSe<sub>2</sub>, and WS<sub>2</sub>/MoSe<sub>2</sub> heterostructure regions, respectively. For all areas, the PL decays are fit by a two-component exponential decay, namely, a

fast decay  $\tau_1$  and a slow decay  $\tau_2$ . From the data shown in Figure 1F, we obtain a fast decay lifetime of 32 and 44 ps for WS<sub>2</sub> and MoSe<sub>2</sub>, respectively, which is similar to the transient absorption measurements of other monolayer TMD materials.<sup>46</sup> The fast decay component is attributed to exciton recombination, which takes up a percentage of higher than 98% (Table S1), indicating that the radiative recombination channel of the A exciton is

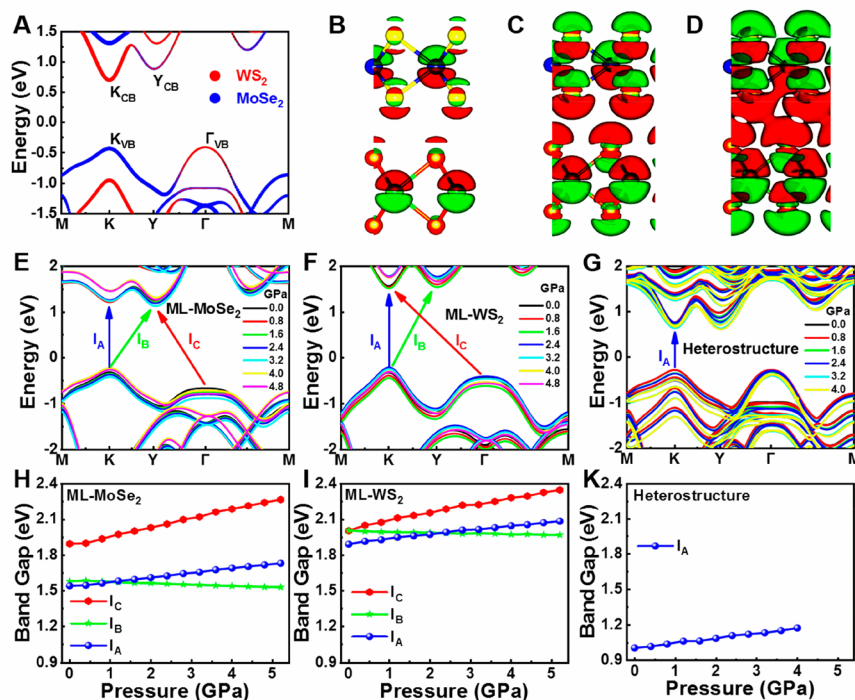


**Figure 4.** Calculated band structure and differential charge density of the WS<sub>2</sub>/MoSe<sub>2</sub> heterobilayer under external pressure. (A) Calculated band structure of the WS<sub>2</sub>/MoSe<sub>2</sub> heterobilayer. The relative contribution from each layer (MoSe<sub>2</sub> and WS<sub>2</sub>, denoted by the blue and red dot, respectively) is represented by the size of the symbols. (B–D) Differential charge density of the WS<sub>2</sub>/MoSe<sub>2</sub> heterobilayer when the external pressure is 0.7, 2.0, and 4.0 GPa, respectively (red = positive, green = negative, isosurface level = 0.005). (E, F) Calculated band structure of ML-MoSe<sub>2</sub> and ML-WS<sub>2</sub> under external pressure, respectively. (G) Electronic band structures of WS<sub>2</sub>/MoSe<sub>2</sub> heterobilayers as a function of external pressure in the range 0–4.0 GPa. (H–K) Calculated band gap of typical electronic band transitions in the momentum space (marked in parts E–G, respectively) as a function of external pressure.

dominant. Furthermore, the fast decay lifetime of 93 ps for the WS<sub>2</sub>/MoSe<sub>2</sub> heterostructure, obtained using a 750 nm long-pass filter, is significantly longer than the decay of individual WS<sub>2</sub> and MoSe<sub>2</sub>, which is attributed to the lifetime of interlayer exciton and is comparable with previously reported values.<sup>43</sup> The slow decay component has a lifetime of ~418, 604, and 774 ps for WS<sub>2</sub>, MoSe<sub>2</sub>, and the WS<sub>2</sub>/MoSe<sub>2</sub> heterostructure, respectively, which could be attributed to either different localization of the charge carriers<sup>46</sup> or cooling off the lattice.<sup>47</sup>

Subsequently, we investigated the pressure effect on both the intralayer and interlayer excitonic states at monolayer and heterostructure regions, respectively (Figures 2 and 3). The experiment setup is shown in Figure 3A, which combined a micro-PL system with a DAC device that is capable of implementing high pressure on the sample transferred on diamond. By adjusting the DAC device manually and using the PL peak position of a ruby as a calibration of pressure, various pressures can be effectively applied on the sample. The arrangement on the right side of Figure 3A accords with the most stable stack structure in theoretical calculations (2H stacking) (Figure S3 and Table S2).

Parts A–C of Figure 2 show the typical PL spectra of ML-MoSe<sub>2</sub>, the WS<sub>2</sub>/MoSe<sub>2</sub> heterostructure, and ML-WS<sub>2</sub> under various pressures. When hydrostatic pressure was applied to ML-MoSe<sub>2</sub>, ML-WS<sub>2</sub>, and the WS<sub>2</sub>/MoSe<sub>2</sub> heterostructure, respectively, the emission intensities of their PL peaks all decreased. Inspired by the previous reports in MoS<sub>2</sub> systems,<sup>38,48,49</sup> the PL results for ML-WS<sub>2</sub> and ML-MoSe<sub>2</sub> here may be correlated with the pressure-induced direct-to-indirect band transition, which would decrease the PL quantum

yield and thus lower the emission intensities dramatically. The intensity of the IX peak nearly vanishes under 8.9 GPa, which can be explained by pressure-induced direct-to-indirect transition and the reduced excitonic absorption (Figure S4).

In contrast to monolayer TMDs, the IX peak of the WS<sub>2</sub>/MoSe<sub>2</sub> heterostructure exhibited relatively more sophisticated evolution with pressure, because it not only corresponds to the electronic structure of both components but also depends on the interlayer coupling.<sup>50</sup> Therefore, we systematically investigated the PL spectra of the WS<sub>2</sub>/MoSe<sub>2</sub> heterostructure with pressure ranging from 0 to 8.9 GPa. As seen in Figure 2D,E, the intensity of IX and X<sub>WS<sub>2</sub></sub> (normalized by IX intensity) in heterostructure exhibits strong pressure dependence. First, we observed gradual suppression of the X<sub>WS<sub>2</sub></sub> peak in the PL spectrum of the heterostructure compared with IX with increasing pressure. Interestingly, this X<sub>WS<sub>2</sub></sub> peak totally disappeared and only the IX peak remained in the PL spectrum of the heterostructure as the pressure increased to 8.9 GPa. This illustrates the transformation of the major PL emission from intralayer exciton to interlayer exciton in this heterostructure system. That is, the interlayer coupling of vdW heterostructure can be effectively enhanced by applying external pressure.

We further define  $R$  as the intensity ratio of the IX peak and the X<sub>WS<sub>2</sub></sub> exciton peak ( $P_{IX}/P_{X_{WS_2}}$ ) to trace the trend of PL peaks with increasing pressure (Table S3). Here, for the initial pressure at nearly zero, we note that  $P_{X_{WS_2}}$  (exciton emission intensity) is typically 2–3 times stronger than  $P_{IX}$  (interlayer exciton emission intensity), possibly due to the relatively weak interlayer coupling and indirect nature of interlayer excitons. Through

statistical analysis, the ratio  $R$  is from 1:2.6 at 0 GPa to 1:0.3 at 3.8 GPa. It is notable that at 8.9 GPa only the emission of interlayer excitons was detectable in the PL spectrum, indicating that interlayer exciton emission is more robust under higher pressure. Therefore, the trend of the ratio  $R$  can directly reflect the tuning of interlayer electronic coupling strength under various pressures: the higher the ratio, the stronger the coupling strength. As shown on the right side of Figure 3A, the proportion of interlayer excitons is gradually enhanced with increasing pressure and finally totally governs the emission of heterostructure.

Besides, the peak width of interlayer excitons also shows a significant increase once pressure is applied (Figure 2D). We consider two possible mechanisms: (1) As seen from the pressure-dependent absorption spectra (Figure S4), the excitonic absorption decreased and gradually evolved toward band edge absorption with increasing pressure, which will lead to a broadened PL spectra. (2) The enhanced photon-mediated intervalley scattering rate,<sup>51</sup> due to direct-to-indirect transition (Figure 4G), will contribute to the spectral broadening. Nevertheless, specific identification of different components of the interlayer exciton peak needs further experiments at lower temperature. Above all, using PL as a probe, we have achieved strong tuning of interlayer electronic coupling strength via external pressure.

Not only the electronic coupling strength but also the electronic structure can be tuned by pressure, which provides us a good opportunity to study the nature of the interlayer exciton of the WS<sub>2</sub>/MoSe<sub>2</sub> heterostructure. We have concluded that the electronic coupling strength was largely enhanced under high pressure. To better understand the effects of high pressure on the electronic structure, we carefully analyzed the corresponding emission peak energy of ML-MoSe<sub>2</sub>, ML-WS<sub>2</sub>, and the WS<sub>2</sub>/MoSe<sub>2</sub> heterostructure under pressure. As shown in Figure 3B,D, it is clear that the blue-shifts of the PL peaks of both ML-MoSe<sub>2</sub> and ML-WS<sub>2</sub> were observed as the pressure was increasing. This energy shift may be related to bandgap tuning by pressure.<sup>38</sup> The peak energy evolution of A<sub>MoSe<sub>2</sub></sub> and A<sub>WS<sub>2</sub></sub> as a function of pressure is performed in Figure 3E and shows a linear increase at a rate of 19.8 and 9.3 meV/GPa, respectively. This behavior is consistent with previous work on ML-MoSe<sub>2</sub>,<sup>38,48</sup> which had shown that the PL peak exhibited a blue-shift with pressure. Moreover, previous theoretical calculation indicates that the K valley of the conduction band will shift upward under a compressive strain in agreement with our calculations.<sup>52–54</sup> Interestingly, by comparing the pressure effect on the A exciton energies of the ML-MoSe<sub>2</sub> and ML-WS<sub>2</sub>, the interlayer exciton energy only shows weak pressure dependence, which was significantly different from the high-pressure response of other bilayer TMD samples. For example, the indirect interband transition of bilayer MoS<sub>2</sub> exhibits complex evolution.<sup>48</sup> Multiple measurements were performed to verify the repeatability of the results, and the results of one of the repeated measurements are shown in Figure S5. The nonsensitive behavior of the interlayer exciton energy could be due to the following two factors: (1) the conduction band edge of WS<sub>2</sub> and valence band edge of MoSe<sub>2</sub> shift to the same direction with comparative rate, and the energy of the interlayer exciton transition corresponding to them could keep almost the same value or only display weak dependence; (2) it is possible that hybridization bands<sup>31</sup> exist near the band edge of both components and they are not sensitive to pressure.

We have also performed the reflectance contrast and Raman measurements of the WS<sub>2</sub>/MoSe<sub>2</sub> heterostructure under high pressure (Figures S4 and S6). Three peaks, i.e., IX, B<sub>MoSe<sub>2</sub></sub>, and A<sub>WS<sub>2</sub></sub>, were clearly observed in the reflectance contrast spectrum. From Figure S4, we can see that the energies of the peaks B<sub>MoSe<sub>2</sub></sub> (B exciton of ML-MoSe<sub>2</sub>) and A<sub>WS<sub>2</sub></sub> all show a blue-shift with pressure, whereas the peak IX only shows a weak pressure dependence, which is consistent with our PL result. Besides, it is obvious that the excitonic absorption gradually decreased and broadened with pressure, which leads to the observed spectrally broadened PL measurements. In addition, it can be seen from the Raman measurement (Figure S6) that both the out-of-plane vibration mode A<sub>1g</sub> and the in-plane vibration mode E<sup>1</sup><sub>2g</sub> show a weak blue-shift phenomenon with pressure, which indicates that the pressure has a certain effect on the interlayer coupling and in-plane lattice change.

To better understand the effects of high pressure on the electronic coupling and electronic structure, we conducted density functional theory (DFT) calculations. The calculated band structure and partial charge density (Figures 4A and S7) show that the valence band maximum (VBM) and conduction band minimum (CBM) of the WS<sub>2</sub>/MoSe<sub>2</sub> heterostructure originate from the MoSe<sub>2</sub> and WS<sub>2</sub> layers, respectively. From the differential charge density in Figure 4B–D, it can be seen that, as the pressure gradually increases, the coupling strength gradually increases, which is in good agreement with our experimental results: at 0 GPa, when the coupling strength is relatively weak, the emission of heterostructure is dominated by ML-WS<sub>2</sub>, while, with increasing coupling strength under higher pressure, the emission of interlayer excitons becomes gradually dominant; at 8.9 GPa, the emission of WS<sub>2</sub> is totally suppressed and the emission of IX totally governs the heterostructure PL spectrum. In addition, we have confirmed through DFT calculations that the band gaps of ML-MoSe<sub>2</sub> (Figure 4E,H), ML-WS<sub>2</sub> (Figure 4F, I), and the WS<sub>2</sub>/MoSe<sub>2</sub> heterostructure all change from direct band gaps to indirect band gaps with the increase of pressure. The WS<sub>2</sub>/MoSe<sub>2</sub> heterobilayer is known to exhibit a type-II band alignment with the CBM (VBM) located at the K (K) point. In a heterobilayer with relative weak interlayer interaction, both intralayer and interlayer exciton emissions from individual layers can be observed, which is different from the WSe<sub>2</sub>–MoSe<sub>2</sub> heterobilayer.<sup>50</sup> With increasing interlayer interaction strength, the efficient charge separation process can lead to exclusive emissions from interlayer excitons formed by electrons and holes from different layers.<sup>30</sup> Specifically, in free heterobilayer WS<sub>2</sub>/MoSe<sub>2</sub> (Figure 4G), the VBM is at the K point. The band gap of heterobilayer WS<sub>2</sub>/MoSe<sub>2</sub> is very sensitive to pressure, and very small pressure can make it from direct to indirect band gap. As pressure increases, a band changeover occurs and the VBM changes from K to  $\Gamma$  (Figure S8).

In addition, previous calculations show that the hybridized d<sub>x<sup>2</sup>-y<sup>2</sup></sub> and d<sub>xy</sub> orbitals dominate the VBM of monolayer transition metal dichalcogenides, while the d<sub>z<sup>2</sup></sub> orbitals dominate the CBM. The similar orbital contribution from metal atoms dominates the heterostructure WS<sub>2</sub>/MoSe<sub>2</sub> as well (Figure S7). The orbital overlapping of the sulfur and selenium atoms is strongly dependent on the interlayer distance. When the external pressure increases, the enhanced interlayer coupling leads to strong interaction of chalcogenide atoms while leaving a negligible interaction between metal atoms. Thus, the direct

interlayer hopping remains almost intact but the indirect interlayer hopping dominates, leading to the changeover between direct band gap and indirect band gap. Intriguingly, the applied pressure for the band changeover of the WS<sub>2</sub>/MoSe<sub>2</sub> heterostructure is much smaller than that for individual monolayer material.

## CONCLUSION

In summary, we have effectively tuned the electronic structure and interlayer coupling in the high-quality WS<sub>2</sub>/MoSe<sub>2</sub> heterostructure in a quantitative way, by applying hydrostatic pressure via diamond anvil cell. First, we obtained a high-quality WS<sub>2</sub>/MoSe<sub>2</sub> heterostructure on diamond by dry transfer and annealing under a vacuum. The intralayer exciton energy of both ML-MoSe<sub>2</sub> and ML-WS<sub>2</sub> shows a clear blue-shift, while the interlayer exciton energy only shows weak pressure dependence, significantly different from the high pressure response of other bilayer TMD samples. For this phenomenon, we propose two possible explanations: First, the conduction band edge of WS<sub>2</sub> and the valence band edge of MoSe<sub>2</sub> shifts to the same direction with comparable rate; second, it is possible that hybridization bands exist near the band edge of both components and they are not sensitive to pressure. Theoretical calculation reveals the enhanced interlayer interaction via the chalcogenide atoms, which is consistent with the observed enhanced ratio of IX/X<sub>WS<sub>2</sub></sub> PL intensity at the heterostructure region (corresponded to enhanced interlayer excitons). Meanwhile, theoretical calculation also provides the signature of pressure-induced direct–indirect band gap transition in ML-MoSe<sub>2</sub>, ML-WS<sub>2</sub>, and the WS<sub>2</sub>/MoSe<sub>2</sub> heterostructure, which could affect the PL intensity of individual monolayers and heterostructures as well. Our work has provided a good way to understand the correlation between interlayer interaction and electronic/optical properties in atomic-level vdW heterostructures, which is beneficial for electronic device design from the large quantum material family and their potential applications.

## ASSOCIATED CONTENT

### Supporting Information

The Supporting Information is available free of charge at <https://pubs.acs.org/doi/10.1021/acs.nanolett.1c02281>.

Materials and methods; a photograph of the sample preparation process; PL spectra of ML-MoSe<sub>2</sub>, ML-WS<sub>2</sub>, and WS<sub>2</sub>/MoSe<sub>2</sub> heterostructures; PL lifetime and corresponding percentum of ML-MoSe<sub>2</sub>, ML-WS<sub>2</sub>, and WS<sub>2</sub>/MoSe<sub>2</sub> heterostructures; the top and side views of the WS<sub>2</sub>/MoSe<sub>2</sub> heterobilayer with high-symmetry stacking structures; the binding energy  $E_b$  of bilayer WS<sub>2</sub>/MoSe<sub>2</sub> heterobilayers with different stacking configurations; the reflectance contrast spectra of the WS<sub>2</sub>/MoSe<sub>2</sub> heterostructure under different pressures; the intensity ratio of the IX peak and the A exciton peak with different pressures; pressure-dependent PL spectra of the WS<sub>2</sub>/MoSe<sub>2</sub> heterostructure; the Raman spectra of the WS<sub>2</sub>/MoSe<sub>2</sub> heterostructure under different pressures; the calculated partial charge density of the WS<sub>2</sub>/MoSe<sub>2</sub> heterobilayer; the pressure-dependent band structures of the WS<sub>2</sub>/MoSe<sub>2</sub> heterobilayer including spin–orbit coupling (PDF)

## AUTHOR INFORMATION

### Corresponding Authors

**Fang Hong** – Beijing National Laboratory for Condensed Matter Physics, Institute of Physics, Chinese Academy of Sciences, Beijing 100190, China; University of Chinese Academy of Sciences, Beijing 100049, China; Songshan Lake Materials Laboratory, Dongguan, Guangdong 523808, China; Email: [hongfang@iphy.ac.cn](mailto:hongfang@iphy.ac.cn)

**Jiatao Sun** – School of Information and Electronics, MIIT Key Laboratory for Low-Dimensional Quantum Structure and Devices, Beijing Institute of Technology, Beijing 100081, China; Email: [jtsun@bit.edu.cn](mailto:jtsun@bit.edu.cn)

**Xiaoxian Zhang** – Key Laboratory of Luminescence and Optical Information, Ministry of Education, Institute of Optoelectronic Technology, Beijing Jiaotong University, Beijing 100044, China; [orcid.org/0000-0002-4215-8274](https://orcid.org/0000-0002-4215-8274); Email: [zhxiaoxian@bjtu.edu.cn](mailto:zhxiaoxian@bjtu.edu.cn)

**Xiaohui Yu** – Beijing National Laboratory for Condensed Matter Physics, Institute of Physics, Chinese Academy of Sciences, Beijing 100190, China; University of Chinese Academy of Sciences, Beijing 100049, China; Songshan Lake Materials Laboratory, Dongguan, Guangdong 523808, China; [orcid.org/0000-0001-8880-2304](https://orcid.org/0000-0001-8880-2304); Email: [yuxh@iphy.ac.cn](mailto:yuxh@iphy.ac.cn)

### Authors

**Xiaoli Ma** – Beijing National Laboratory for Condensed Matter Physics, Institute of Physics, Chinese Academy of Sciences, Beijing 100190, China; [orcid.org/0000-0002-8835-4684](https://orcid.org/0000-0002-8835-4684)

**Shaohua Fu** – Key Laboratory of Luminescence and Optical Information, Ministry of Education, Institute of Optoelectronic Technology, Beijing Jiaotong University, Beijing 100044, China

**Jianwei Ding** – CAS Key Laboratory of Standardization and Measurement for Nanotechnology, CAS Center for Excellence in Nanoscience, National Center for Nanoscience and Technology, Beijing 100190, China; University of Chinese Academy of Sciences, Beijing 100049, China

**Meng Liu** – School of Information and Electronics, MIIT Key Laboratory for Low-Dimensional Quantum Structure and Devices, Beijing Institute of Technology, Beijing 100081, China

**Ang Bian** – Key Laboratory of Luminescence and Optical Information, Ministry of Education, Institute of Optoelectronic Technology, Beijing Jiaotong University, Beijing 100044, China

**Dawei He** – Key Laboratory of Luminescence and Optical Information, Ministry of Education, Institute of Optoelectronic Technology, Beijing Jiaotong University, Beijing 100044, China

Complete contact information is available at: <https://pubs.acs.org/doi/10.1021/acs.nanolett.1c02281>

### Author Contributions

∇X.M., S.F., J.D., and M.L. contributed equally to this work. F.H., X.Y., and X.Z. conceived the study. J.D. prepared the sample. X.M. loaded and pressurized the sample. X.M. carried out the Raman, PL, and reflectance contrast measurements. S.F. performed the TRPL measurements. J.S. and M.L. calculated the band structures. X.M. and S.F. wrote and revised the manuscript. F.H., J.S., X.Z., D.H., and X.Y. participated in revising the manuscript. All authors discussed the results.

## Notes

The authors declare no competing financial interest.

## ACKNOWLEDGMENTS

This work was supported by the National Key Research and Development Program of China (2016YFA0401503, 2018YFA0305700, 2016YFA0202302, 2020YFA0308800, and 2016YFA0202300), the National Natural Science Foundation of China (NSFC 11974088, 61875236, 61975007, 61527817, 11974045, and 11575288), the Beijing Natural Science Foundation (Grant No. Z190006), the Strategic Priority Research Program and Key Research Program of Frontier Sciences of the Chinese Academy of Sciences (Grant Nos. XDB30000000, XDB33000000, XDB25000000, and QYZDBSSW-SLH013), and the Youth Innovation Promotion Association of Chinese Academy of Sciences (Grant No. Y202003).

## REFERENCES

- (1) Yuan, H.; Bahramy, M. S.; Morimoto, K.; Wu, S.; Nomura, K.; Yang, B.-J.; Shimotani, H.; Suzuki, R.; Toh, M.; Kloc, C.; Xu, X.; Arita, R.; Nagaosa, N.; Iwasa, Y. Zeeman-type spin splitting controlled by an electric field. *Nat. Phys.* **2013**, *9* (9), 563–569.
- (2) Wang, H.; Lu, Z.; Xu, S.; Kong, D.; Cha, J. J.; Zheng, G.; Hsu, P. C.; Yan, K.; Bradshaw, D.; Prinz, F. B.; Cui, Y. Electrochemical tuning of vertically aligned MoS<sub>2</sub> nanofilms and its application in improving hydrogen evolution reaction. *Proc. Natl. Acad. Sci. U. S. A.* **2013**, *110* (49), 19701–6.
- (3) Sun, L.; Yan, J.; Zhan, D.; Liu, L.; Hu, H.; Li, H.; Tay, B. K.; Kuo, J. L.; Huang, C. C.; Hewak, D. W.; Lee, P. S.; Shen, Z. X. Spin-orbit splitting in single-layer MoS<sub>2</sub> revealed by triply resonant Raman scattering. *Phys. Rev. Lett.* **2013**, *111* (12), 126801.
- (4) Jin, W.; Yeh, P. C.; Zaki, N.; Zhang, D.; Sadowski, J. T.; Al-Mahboob, A.; van der Zande, A. M.; Chenet, D. A.; Dadap, J. I.; Herman, I. P.; Sutter, P.; Hone, J.; Osgood, R. M., Jr. Direct measurement of the thickness-dependent electronic band structure of MoS<sub>2</sub> using angle-resolved photoemission spectroscopy. *Phys. Rev. Lett.* **2013**, *111* (10), 106801.
- (5) Komsa, H. P.; Kotakoski, J.; Kurasch, S.; Lehtinen, O.; Kaiser, U.; Krasheninnikov, A. V. Two-dimensional transition metal dichalcogenides under electron irradiation: defect production and doping. *Phys. Rev. Lett.* **2012**, *109* (3), 035503.
- (6) Wang, Q. H.; Kalantar-Zadeh, K.; Kis, A.; Coleman, J. N.; Strano, M. S. Electronics and optoelectronics of two-dimensional transition metal dichalcogenides. *Nat. Nanotechnol.* **2012**, *7* (11), 699–712.
- (7) Tongay, S.; Zhou, J.; Ataca, C.; Lo, K.; Matthews, T. S.; Li, J.; Grossman, J. C.; Wu, J. Thermally driven crossover from indirect toward direct bandgap in 2D semiconductors: MoSe<sub>2</sub> versus MoS<sub>2</sub>. *Nano Lett.* **2012**, *12* (11), 5576–80.
- (8) Yuan, H.; Wang, X.; Lian, B.; Zhang, H.; Fang, X.; Shen, B.; Xu, G.; Xu, Y.; Zhang, S. C.; Hwang, H. Y.; Cui, Y. Generation and electric control of spin-valley-coupled circular photogalvanic current in WSe<sub>2</sub>. *Nat. Nanotechnol.* **2014**, *9* (10), 851–7.
- (9) Qiu, D. Y.; da Jornada, F. H.; Louie, S. G. Optical spectrum of MoS<sub>2</sub>: many-body effects and diversity of exciton states. *Phys. Rev. Lett.* **2013**, *111* (21), 216805.
- (10) Mak, K. F.; Lee, C.; Hone, J.; Shan, J.; Heinz, T. F. Atomically thin MoS<sub>2</sub>: a new direct-gap semiconductor. *Phys. Rev. Lett.* **2010**, *105* (13), 136805.
- (11) Splendiani, A.; Sun, L.; Zhang, Y.; Li, T.; Kim, J.; Chim, C. Y.; Galli, G.; Wang, F. Emerging photoluminescence in monolayer MoS<sub>2</sub>. *Nano Lett.* **2010**, *10* (4), 1271–5.
- (12) Zhang, Y.; Chang, T. R.; Zhou, B.; Cui, Y. T.; Yan, H.; Liu, Z.; Schmitt, F.; Lee, J.; Moore, R.; Chen, Y.; Lin, H.; Jeng, H. T.; Mo, S. K.; Hussain, Z.; Bansil, A.; Shen, Z. X. Direct observation of the transition from indirect to direct bandgap in atomically thin epitaxial MoSe<sub>2</sub>. *Nat. Nanotechnol.* **2014**, *9* (2), 111–5.
- (13) Xiao, D.; Liu, G. B.; Feng, W.; Xu, X.; Yao, W. Coupled spin and valley physics in monolayers of MoS<sub>2</sub> and other group-VI dichalcogenides. *Phys. Rev. Lett.* **2012**, *108* (19), 196802.
- (14) Zeng, H.; Dai, J.; Yao, W.; Xiao, D.; Cui, X. Valley polarization in MoS<sub>2</sub> monolayers by optical pumping. *Nat. Nanotechnol.* **2012**, *7* (8), 490–3.
- (15) Mak, K. F.; He, K.; Shan, J.; Heinz, T. F. Control of valley polarization in monolayer MoS<sub>2</sub> by optical helicity. *Nat. Nanotechnol.* **2012**, *7* (8), 494–8.
- (16) Mak, K. F.; He, K.; Lee, C.; Lee, G. H.; Hone, J.; Heinz, T. F.; Shan, J. Tightly bound trions in monolayer MoS<sub>2</sub>. *Nat. Mater.* **2013**, *12* (3), 207–11.
- (17) Chernikov, A.; Berkelbach, T. C.; Hill, H. M.; Rigosi, A.; Li, Y.; Aslan, O. B.; Reichman, D. R.; Hybertsen, M. S.; Heinz, T. F. Exciton binding energy and nonhydrogenic Rydberg series in monolayer WS<sub>2</sub>. *Phys. Rev. Lett.* **2014**, *113* (7), 076802.
- (18) He, K.; Kumar, N.; Zhao, L.; Wang, Z.; Mak, K. F.; Zhao, H.; Shan, J. Tightly bound excitons in monolayer WSe<sub>2</sub>. *Phys. Rev. Lett.* **2014**, *113* (2), 026803.
- (19) Li, M.-Y.; Chen, C.-H.; Shi, Y.; Li, L.-J. Heterostructures based on two-dimensional layered materials and their potential applications. *Mater. Today* **2016**, *19* (6), 322–335.
- (20) Geim, A. K.; Grigorieva, I. V. Van der Waals heterostructures. *Nature* **2013**, *499* (7459), 419–25.
- (21) Liu, Y.; Weiss, N. O.; Duan, X.; Cheng, H.-C.; Huang, Y.; Duan, X. Van der Waals heterostructures and devices. *Nat. Rev. Mater.* **2016**, *1* (9), 16042.
- (22) Novoselov, K. S.; Mishchenko, A.; Carvalho, A.; Neto, A. H. C. 2D materials and van Der Waals heterostructures. *Science* **2016**, *353*, aac9439.
- (23) Ponomarenko, L. A.; Gorbachev, R. V.; Yu, G. L.; Elias, D. C.; Jalil, R.; Patel, A. A.; Mishchenko, A.; Mayorov, A. S.; Woods, C. R.; Wallbank, J. R.; Mucha-Kruczynski, M.; Piot, B. A.; Potemski, M.; Grigorieva, I. V.; Novoselov, K. S.; Guinea, F.; Fal'ko, V. I.; Geim, A. K. Cloning of Dirac fermions in graphene superlattices. *Nature* **2013**, *497* (7451), 594–7.
- (24) Hunt, B.; Sanchez-Yamagishi, J. D.; Young, A. F.; Yankowitz, M.; LeRoy, B. J.; Watanabe, K.; Taniguchi, T.; Moon, P.; Koshino, M.; Jarillo-Herrero, P. Massive Dirac fermions and Hofstadter butterfly in a van der Waals heterostructure. *Science* **2013**, *340* (6139), 1427–1430.
- (25) Dean, C. R.; Wang, L.; Maher, P.; Forsythe, C.; Ghahari, F.; Gao, Y.; Katoch, J.; Ishigami, M.; Moon, P.; Koshino, M.; Taniguchi, T.; Watanabe, K.; Shepard, K. L.; Hone, J.; Kim, P. Hofstadter's butterfly and the fractal quantum Hall effect in moire superlattices. *Nature* **2013**, *497* (7451), 598–602.
- (26) Spanton, E. M.; Zibrov, A. A.; Zhou, H.; Taniguchi, T.; Watanabe, K.; Zaletel, M. P.; Young, A. F. Observation of fractional Chern insulators in a van der Waals heterostructure. *Science* **2018**, *360* (6384), 62–66.
- (27) Cao, Y.; Fatemi, V.; Fang, S.; Watanabe, K.; Taniguchi, T.; Kaxiras, E.; Jarillo-Herrero, P. Unconventional superconductivity in magic-angle graphene superlattices. *Nature* **2018**, *556* (7699), 43–50.
- (28) Cao, Y.; Fatemi, V.; Demir, A.; Fang, S.; Tomarken, S. L.; Luo, J. Y.; Sanchez-Yamagishi, J. D.; Watanabe, K.; Taniguchi, T.; Kaxiras, E.; Ashoori, R. C.; Jarillo-Herrero, P. Correlated insulator behaviour at half-filling in magic-angle graphene superlattices. *Nature* **2018**, *556* (7699), 80–84.
- (29) Chen, G.; Jiang, L.; Wu, S.; Lyu, B.; Li, H.; Chittari, B. L.; Watanabe, K.; Taniguchi, T.; Shi, Z.; Jung, J.; Zhang, Y.; Wang, F. Evidence of a gate-tunable Mott insulator in a trilayer graphene moiré superlattice. *Nat. Phys.* **2019**, *15* (3), 237–241.
- (30) Jin, C.; Regan, E. C.; Yan, A.; Iqbal Bakti Utama, M.; Wang, D.; Zhao, S.; Qin, Y.; Yang, S.; Zheng, Z.; Shi, S.; Watanabe, K.; Taniguchi, T.; Tongay, S.; Zettl, A.; Wang, F. Observation of moire excitons in WSe<sub>2</sub>/WS<sub>2</sub> heterostructure superlattices. *Nature* **2019**, *567* (7746), 76–80.
- (31) Alexeev, E. M.; Ruiz-Tijerina, D. A.; Danovich, M.; Hamer, M. J.; Terry, D. J.; Nayak, P. K.; Ahn, S.; Pak, S.; Lee, J.; Sohn, J. I.; Molas, M. R.; Koperski, M.; Watanabe, K.; Taniguchi, T.; Novoselov, K. S.;

Gorbachev, R. V.; Shin, H. S.; Fal'ko, V. I.; Tartakovskii, A. I. Resonantly hybridized excitons in moiré superlattices in van der Waals heterostructures. *Nature* **2019**, *567* (7746), 81–86.

(32) Gong, C.; Zhang, H.; Wang, W.; Colombo, L.; Wallace, R. M.; Cho, K. Band alignment of two-dimensional transition metal dichalcogenides: Application in tunnel field effect transistors. *Appl. Phys. Lett.* **2013**, *103* (5), 053513.

(33) Kang, J.; Tongay, S.; Zhou, J.; Li, J.; Wu, J. Band offsets and heterostructures of two-dimensional semiconductors. *Appl. Phys. Lett.* **2013**, *102* (1), 012111.

(34) Tongay, S.; Fan, W.; Kang, J.; Park, J.; Koldemir, U.; Suh, J.; Narang, D. S.; Liu, K.; Ji, J.; Li, J.; Sinclair, R.; Wu, J. Tuning interlayer coupling in large-area heterostructures with CVD-grown MoS<sub>2</sub> and WS<sub>2</sub> monolayers. *Nano Lett.* **2014**, *14* (6), 3185–90.

(35) Fang, H.; Battaglia, C.; Carraro, C.; Nemsak, S.; Ozdol, B.; Kang, J. S.; Bechtel, H. A.; Desai, S. B.; Kronast, F.; Unal, A. A. Strong interlayer coupling in van der Waals heterostructures built from single-layer chalcogenides. *Proc. Natl. Acad. Sci. U. S. A.* **2014**, *111* (17), 6198–6202.

(36) Liu, K.; Zhang, L.; Cao, T.; Jin, C.; Qiu, D.; Zhou, Q.; Zettl, A.; Yang, P.; Louie, S. G.; Wang, F. Evolution of interlayer coupling in twisted molybdenum disulfide bilayers. *Nat. Commun.* **2014**, *5*, 4966.

(37) Chi, Z. H.; Zhao, X. M.; Zhang, H.; Goncharov, A. F.; Lobanov, S. S.; Kagayama, T.; Sakata, M.; Chen, X. J. Pressure-induced metallization of molybdenum disulfide. *Phys. Rev. Lett.* **2014**, *113* (3), 036802.

(38) Fu, L.; Wan, Y.; Tang, N.; Ding, Y.-m.; Gao, J.; Yu, J.; Guan, H.; Zhang, K.; Wang, W.; Zhang, C. K-Λ crossover transition in the conduction band of monolayer MoS<sub>2</sub> under hydrostatic pressure. *Sci. Adv.* **2017**, *3* (11), No. e1700162.

(39) Zhao, Z.; Zhang, H.; Yuan, H.; Wang, S.; Lin, Y.; Zeng, Q.; Xu, G.; Liu, Z.; Solanki, G. K.; Patel, K. D.; Cui, Y.; Hwang, H. Y.; Mao, W. L. Pressure induced metallization with absence of structural transition in layered molybdenum diselenide. *Nat. Commun.* **2015**, *6*, 7312.

(40) Nayak, A. P.; Yuan, Z.; Cao, B.; Liu, J.; Wu, J.; Moran, S. T.; Li, T.; Akinwande, D.; Jin, C.; Lin, J.-F. Pressure-modulated conductivity, carrier density, and mobility of multilayered tungsten disulfide. *ACS Nano* **2015**, *9* (9), 9117–9123.

(41) Nayak, A. P.; Bhattacharyya, S.; Zhu, J.; Liu, J.; Wu, X.; Pandey, T.; Jin, C.; Singh, A. K.; Akinwande, D.; Lin, J. F. Pressure-induced semiconducting to metallic transition in multilayered molybdenum disulfide. *Nat. Commun.* **2014**, *5*, 3731.

(42) Pak, S.; Lee, J.; Lee, Y. W.; Jang, A. R.; Ahn, S.; Ma, K. Y.; Cho, Y.; Hong, J.; Lee, S.; Jeong, H. Y.; Im, H.; Shin, H. S.; Morris, S. M.; Cha, S.; Sohn, J. I.; Kim, J. M. Strain-Mediated Interlayer Coupling Effects on the Excitonic Behaviors in an Epitaxially Grown MoS<sub>2</sub>/WS<sub>2</sub> van der Waals Heterobilayer. *Nano Lett.* **2017**, *17* (9), 5634–5640.

(43) Ceballos, F.; Bellus, M. Z.; Chiu, H. Y.; Zhao, H. Probing charge transfer excitons in a MoSe<sub>2</sub>-WS<sub>2</sub> van der Waals heterostructure. *Nanoscale* **2015**, *7* (41), 17523–8.

(44) Ruiz-Tijerina, D. A.; Fal'ko, V. I. Interlayer hybridization and moiré superlattice minibands for electrons and excitons in heterobilayers of transition-metal dichalcogenides. *Phys. Rev. B: Condens. Matter Mater. Phys.* **2019**, *99* (12), 125424.

(45) Meng, Y.; Wang, T.; Jin, C.; Li, Z.; Miao, S.; Lian, Z.; Taniguchi, T.; Watanabe, K.; Song, F.; Shi, S. F. Electrical switching between exciton dissociation to exciton funneling in MoSe<sub>2</sub>/WS<sub>2</sub> heterostructure. *Nat. Commun.* **2020**, *11* (1), 2640.

(46) Anghel, S.; Passmann, F.; Ruppert, C.; Bristow, A. D.; Betz, M. Coupled exciton-trion spin dynamics in a MoSe<sub>2</sub> monolayer. *2D Mater.* **2018**, *5* (4), 045024.

(47) Ruppert, C.; Chernikov, A.; Hill, H. M.; Rigosi, A. F.; Heinz, T. F. The Role of Electronic and Phononic Excitation in the Optical Response of Monolayer WS<sub>2</sub> after Ultrafast Excitation. *Nano Lett.* **2017**, *17* (2), 644–651.

(48) Dou, X.; Ding, K.; Jiang, D.; Sun, B. Tuning and identification of interband transitions in monolayer and bilayer molybdenum disulfide using hydrostatic pressure. *ACS Nano* **2014**, *8* (7), 7458–7464.

(49) Conley, H. J.; Wang, B.; Ziegler, J. I.; Haglund, R. F., Jr.; Pantelides, S. T.; Bolotin, K. I. Bandgap engineering of strained monolayer and bilayer MoS<sub>2</sub>. *Nano Lett.* **2013**, *13* (8), 3626–30.

(50) Xia, J.; Yan, J.; Wang, Z.; He, Y.; Gong, Y.; Chen, W.; Sum, T. C.; Liu, Z.; Ajayan, P. M.; Shen, Z. Strong coupling and pressure engineering in WSe<sub>2</sub>-MoSe<sub>2</sub> heterobilayers. *Nat. Phys.* **2021**, *17*, 92–98.

(51) Aslan, O. B.; Deng, M.; Heinz, T. F. Strain tuning of excitons in monolayer WSe<sub>2</sub>. *Phys. Rev. B: Condens. Matter Mater. Phys.* **2018**, *98* (11), 115308.

(52) Chang, C.-H.; Fan, X.; Lin, S.-H.; Kuo, J.-L. Orbital analysis of electronic structure and phonon dispersion in MoS<sub>2</sub>, MoSe<sub>2</sub>, WS<sub>2</sub>, and WSe<sub>2</sub> monolayers under strain. *Phys. Rev. B: Condens. Matter Mater. Phys.* **2013**, *88* (19), 195420.

(53) Dong, L.; Dongare, A. M.; Namburu, R. R.; O'Regan, T. P.; Dubey, M. Theoretical study on strain induced variations in electronic properties of 2H-MoS<sub>2</sub> bilayer sheets. *Appl. Phys. Lett.* **2014**, *104* (5), 053107.

(54) Zhao, W.; Ribeiro, R. M.; Toh, M.; Carvalho, A.; Kloc, C.; Castro Neto, A. H.; Eda, G. Origin of indirect optical transitions in few-layer MoS<sub>2</sub>, WS<sub>2</sub>, and WSe<sub>2</sub>. *Nano Lett.* **2013**, *13* (11), 5627–5634.